Journal of Alloys and Compounds 722 (2017) 549–554

Contents lists available at ScienceDirect

Journal of Alloys and Compounds

journal homepage: http://www.elsevier.com/locate/jalcom

On the phase stability of $CaCu_5$-type compounds

M.F.J. Boeije [a, *], E.K. Delczeg-Czirjak [b], N.H. van Dijk [a], O. Eriksson [b], E. Brück [a]

[a] Fundamental Aspects of Materials and Energy, Faculty of Applied Sciences, Delft University of Technology, Mekelweg 15, 2629 JB, Delft, The Netherlands
[b] Division of Materials Theory, Department of Physics and Astronomy, Uppsala University, Box 516, SE-751 20, Uppsala, Sweden

ARTICLE INFO

Article history:
Received 21 February 2017
Received in revised form
2 June 2017
Accepted 12 June 2017
Available online 13 June 2017

Keywords:
Phase stability
Miedema model
$CaCu_5$ prototype

ABSTRACT

We present a hybrid method to inspect the phase stability of compounds having a $CaCu_5$-type crystal structure. This is done using 2D stability plots using the Miedema parameters that are based on the work function and electron density of the constituent elements. Stable compounds are separated from unstable binary compounds, with a probability of 94%. For stable compounds, a linear relation is found, showing a constant ratio of charge transfer and electron density mismatch. DFT calculations show the same trend. Elements from the *s*,*d*,*f*-block are all reliably represented, elements from the *p*-block are still challenging.

1. Introduction

The phase stability of crystal structures is of immense practical importance [1], as the crystallographic phase largely determines the material properties. Materials that crystallize in the $CaCu_5$-type crystal structure [2] (see Fig. 1) are important as permanent magnets [2,3] and are heavily used in metal hydride batteries [4]. This has given rise to a huge number of publications on compounds having this crystal structure, which is reflected in 1600 entries in the Pearson Crystal Database [5]. Extraction of the data on the elemental compositions pertaining this crystal structure can give insight in the stability of the phase. Generally, the combined data extracted from crystallographic databases is used to predict the crystal structure, for a given composition [6]. This is highly relevant for technologically important YFe_5 [7–9]. This composition does not result in the formation of the $CaCu_5$ phase, but instead forms Y_2Fe_{17} and Y_6Fe_{23}. Here we try to answer a more experimentally relevant question: given a certain crystal structure, what compositions are stable?

For intermetallic compounds, the Miedema model can be used to describe the stability based on the enthalpy of the phase compared to the enthalpy of the constituent elements [10]. This semi-empirical approach has proven to show good agreement with experiment [11] and first-principle calculations [12]. In this model, the enthalpy of formation is calculated by considering a cohesive contribution and a destabilizing contribution based on the electron density. The cohesive contribution is based on the difference in work function $\Delta\Phi^*$ of the elements and the electron density difference $\Delta n_{WS}^{1/3}$ is based on the average electron density at the boundary of the Wigner-Seitz cell of the element. The interfacial enthalpy of A surrounded by B is given by

$$\Delta H_{AB} = \frac{V_A^{2/3}}{\left\langle n_{WS}^{1/3}\right\rangle}\left(-P(\Delta\phi^*)^2 + Q\left(\Delta n_{WS}^{1/3}\right)^2 - R\right). \quad (1)$$

where $V_A^{2/3}$ is the contact surface area of A, $\langle n_{WS}^{1/3}\rangle$ is the average electron density, P and Q are dependent on the atomic species and R is a correction term used for metalloid elements. The total enthalpy of formation upon alloying can be determined by taking the concentration c into account:

$$\Delta H = c_A c_B\left(f_B^A \Delta H_{AB} + f_A^B \Delta H_{BA}\right) \quad (2)$$

where f_B^A represents the degree to which A is surrounded by B. The free enthalpy change is approximately equal to the Gibbs free energy change upon alloying. This approach was initially used to describe binary compounds, but was later extended to ternary compounds, by taking the sum of all contributions $\Delta H_{ABC} = \Delta H'_{AB} + \Delta H'_{AC} + \Delta H'_{BC}$ [13,14] where $\Delta H'_{XY}$ takes the composition into account. In this discussion, the value of ΔH does not yield information on the adopted crystal structure and therefore only $\Delta\phi^*$ and $\Delta n_{WS}^{1/3}$ are used as descriptors to describe the phase stability.

* Corresponding author.
E-mail address: m.f.j.boeije@tudelft.nl (M.F.J. Boeije).

http://dx.doi.org/10.1016/j.jallcom.2017.06.134

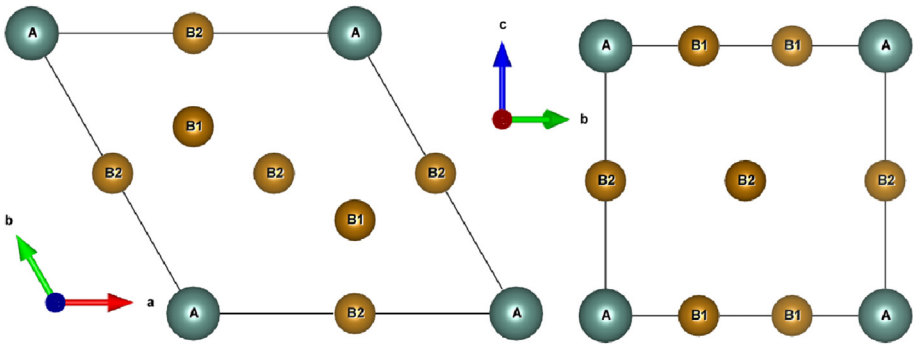

Fig. 1. The unit cell of the $CaCu_5$ type crystal structure with general formula AB_5.

Density functional theory (DFT) calculations do include the crystal structure and can provide the free enthalpy. However, the prediction of a stable compound is not straightforward and the value of the free enthalpy alone does not show the stability of a particular phase. The proper way to do this is to evaluate the global minima of the free enthalpy in a landscape of crystal structures and compositions [15]. Another approach is to analyze existing stable compositions using structure mapping [6,16–18]. This method can be applied to thousands of compositions in seconds, in contrast to the timescales encountered in using DFT methods. In this paper, we present a new approach that combines the semi-empirical parameters that produce accurate results in the Miedema model and the crystallographic data contained in the Pearson database [5]. This is realized by making phase stability plots using $\Delta\phi^*$ and $\Delta n_{WS}^{1/3}$. We extend these values from binary to pseudo-binary compounds by taking the weighted average of the element values. This allows to easily extend these parameters beyond the original scope and without using the experimentally determined P and Q parameters. The obtained stability plots allow for a quick inspection of the phase stability across element combinations. We will show that the application of such a model does not only give a good prediction on phase stability, it also gives valuable information on the factors that govern crystal structure formation in these compounds.

2. Methods

2.1. Computational methods

Three different datasets were extracted from the Pearsons Crystal Database (PCD) [5]. The first is used to assess the predictive power of the parameters used in the Miedema model and contains 3726 entries with unique compositions, by considering all metals without p-type valence electrons. The second is used for the stability of compounds with the $CaCu_5$-type crystal structure, and contains 413 compositions. This number is reduced to 387 when only considering compounds that have a generic formula AB_5. The last set contains $CaCu_5$-derived crystal structures and contains 863 unique compositions. For the stability maps, unstable compounds were generated, based on the assumption that all stable binary compounds have been found. For all entries, compositions containing hydrogen, radioactive elements and actinides were omitted. The position of a compound in the stability map is determined by properties of its atomic constituents. The Miedema parameters Φ and n_{WS} were used [10], including atomic radii [19], listed in the Supplementary information. The weighed properties were normalized $\Omega_w = (a\Omega_A + b\Omega_B)/(a+b)$ for compounds with formula A_aB_b [6]. Within the DFT framework [20,21], the projector augmented wave method as implemented in the Vienna *Ab initio* Simulation Package (VASP) [22–25] was used to generate the total charge and charge densities for ten AB_5 compounds, that is YCu_5, YFe_5, YNi_5, YCo_5, YZn_5, YGa_5 and $BaCu_5$, $CaCu_5$, $MgCu_5$, $SrCu_5$. Exchange-correlation interactions were taken into account via the Perdew- Burke-Ernzerhof type generalized gradient approximation [26]. The 4*s* and 3*d* electrons were treated as valence electrons for Cu, Fe, Ni, Co, Zn. For Y the 4*s*, 4*p*, 5*s*, 4*d*, for Ga the 4*s*, 4*p*, for Mg the 3*s*, for Ca the 3*s*, 3*p*, 4*s*, for Sr the 4*s*, 4*p*, 5*s* and for Ba the 5*s*, 5*p* and 6*s* electrons were treated as valence electrons. The lattice parameters and atomic positions for all compounds were relaxed using the conjugate gradient algorithm until a 0.01 meV/Å force convergence was reached. The plane-wave cutoff and the energy convergence criteria were set to 460 eV and 10^{-8} eV in a $11 \times 11 \times 11(13 \times 13 \times 13)$ Gamma centered k-point mesh for the structural relaxation (charge density calculation).

3. Results and discussion

3.1. Phase stability in binary compounds

The Miedema plots [10] were made using the data obtained from the Pearson database. A total of 628 binary combinations were found with a solubility larger than 7%. Nonradioactive elements were selected from the *s*, *p* and *d* block of the periodic table. Elements from the *p*-block in the periodic system have not been included. Because of the metalloid nature of these elements, an additional term (R) is needed to model the formation enthalpy. A total of 217 unstable compounds was generated based on the available element combinations. The combined data are plotted in Fig. 2.

The plot shows a separation between stable compounds and compounds that do no not form experimentally, illustrated by a demarcation line. There is a separation between compound forming and non-compound forming element combinations when the individual elements have strong dissimilar electronic properties. When elements have similar electronic properties, the separation is less pronounced, especially for $\Delta n_{WS}^{1/3} < 0.2$. For these compounds, the entropy of formation is expected to have a relatively large contribution compared to the enthalpy of formation.

The (configurational) entropy can be kept constant by considering only one crystal structure. For compounds that crystallize in the $CaCu_5$ prototype structure, the configurational entropy is the same and a linear relationship is found between the work function and electron density.

3.2. Phase stability of $CaCu_5$ type compounds

Analogous to the original Miedema plot, the phase stability of a given crystal structure can be investigated. In order to do this, compositions that form the crystal structure in question are plotted

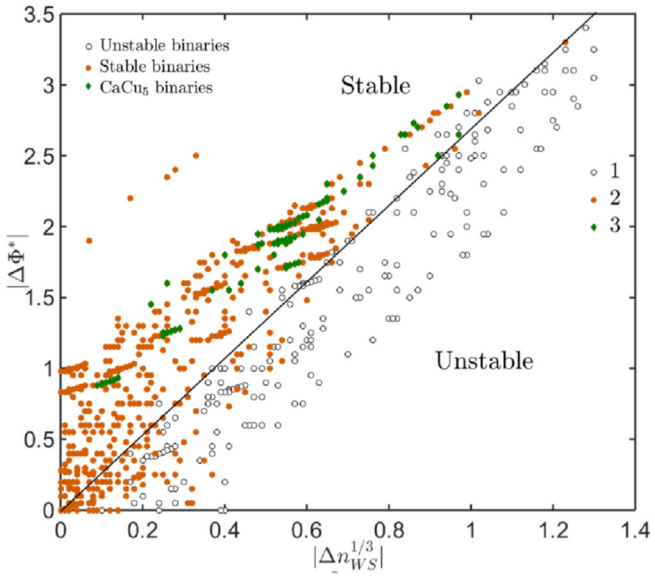

Fig. 2. The difference in work function $|\Delta\Phi^*|$ as a function of the difference in electron density $|\Delta n_{WS}^{1/3}|$ for all binary compounds of *d* metals combined with *s,f* metals. Stable compounds (628 red dots) were extracted from the Pearson database, for cases where the solubility is larger than 7%. Unstable compounds were generated (217 black circles). The black line is a guide to the eye: above it stable compounds are present, while below the black line no compounds are formed. Element combinations that are able to form the $CaCu_5$ crystal structure are indicated with green diamonds and show a linear trend. (For interpretation of the references to colour in this figure legend, the reader is referred to the web version of this article.)

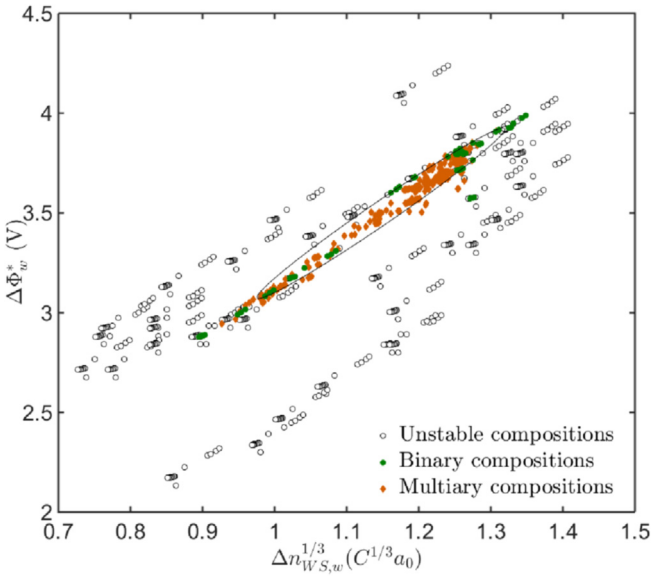

Fig. 4. Phase stability plot of $\Delta\Phi_w^*$ and $\Delta n_{WS,w}^{1/3}$, which are weighted and normalized using the stoichiometry. Green dots and red diamonds represent stable compounds and black circles are generated binary compositions. Binary compositions were complemented with multiary compounds (ternary, quaternary compounds, etc.). The stability region is demarcated by an ellipse. Compounds found outside the ellipse are based on Zn (left) and Pt/Ir (right), and Fe (below). Fe shows a deviation from the linear behavior and is found form a metastable phase (see Supplementary information). The total probability is 94%, based on (3). (For interpretation of the references to colour in this figure legend, the reader is referred to the web version of this article.)

together with compositions that do not form this crystal structure. Assuming that the most common phases of binary compounds have been documented, one can generate a list of unstable binary compositions. By analyzing the occurrence of the various elements in the database, one can reduce the number of unrealistic elemental combinations. This is shown in Fig. 3.

Elements from the *s* and *f* block occupy the A position, while elements from the *d* block occupy the two B positions. The *p*-block elements are also present for some compositions, but they form substitutional alloys and never fully occupy the B positions. The demarcation between A and B is made by La and Y. Early *d*-block elements have been filtered out because they have a different

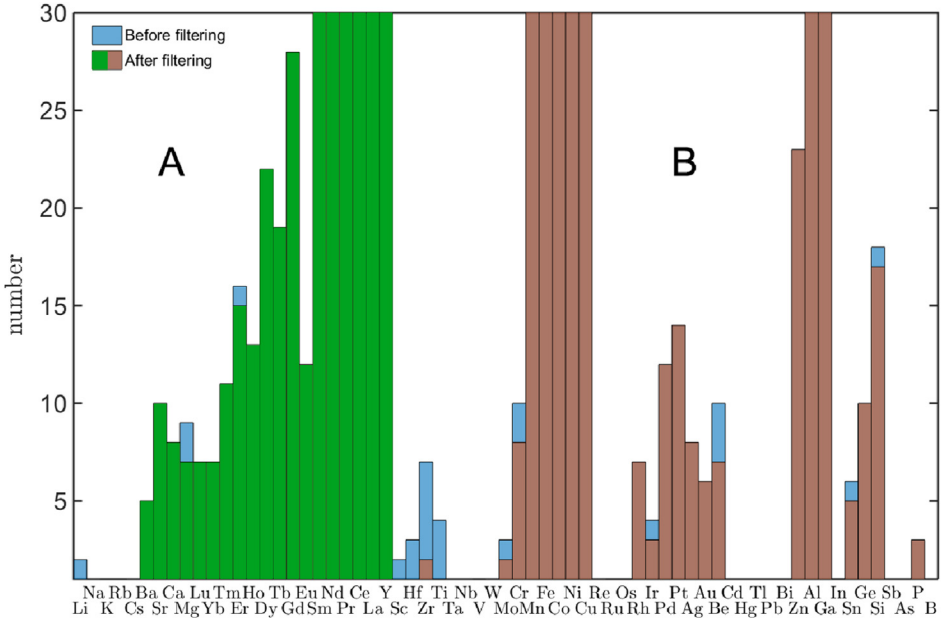

Fig. 3. Histogram of the element combinations forming the $CaCu_5$ crystal structure. Each increment on the *y*-axis is equal to a unique composition. By filtering the raw data by only considering compounds with generic formula AB_5, a strict distinction between elements A and B can be made, indicated in two regions containing green and brown columns respectively. The *x*-axis is based on the Pettifor coordinate and traverses the periodic table first by group and then by period. (For interpretation of the references to colour in this figure legend, the reader is referred to the web version of this article.)

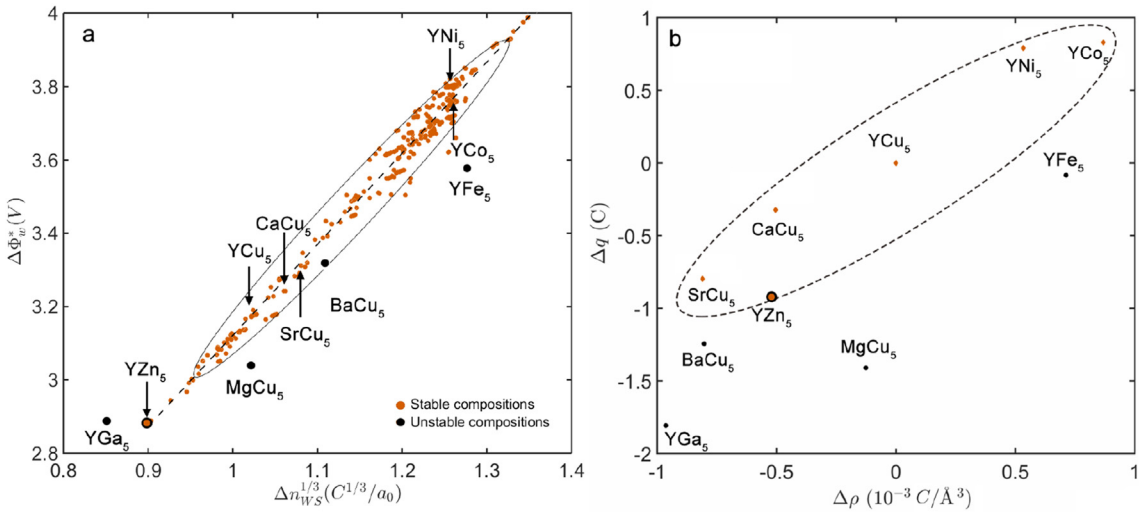

Fig. 5. Electronic characteristics of $CaCu_5$-type compounds based on elemental properties (a) and determined from DFT calculations (b). Both the model in (a) and the DFT calculations in (b) show a linear behavior. The charge q is obtained by integrating the electron density over half the (average) A-B distance. ρ is the average charge density at the same Wigner-Seitz cell radius. Δq and $\Delta\rho$ are determined relative to YCu_5. While $BaCu_5$ is inside the stability region in (a), DFT calculations shows a large charge difference and supports the observation that $BaCu_5$ is unstable. Because there are two reported crystal structures of YZn_5 [28,29], this compound is indicated with a filled circle. The dashed lines are guides to the eye.

stoichiometry or act as dopants.

Using the histogram, all combinations between A and B can be generated and compared to the binary compounds found in the Pearson database. By calculating an average weighted value for the properties of A and B in $(A_{1-x}\ A'_x)(B_{1-y}\ B_y')_5$, it is possible to also include pseudo-binary compounds. This approach has been used earlier [6] and uses an average-atom model [27]. Using such a strategy, Fig. 4 was made, by presenting compounds with up to ten different elements. It contains 387 unique stable compounds and 693 unstable binary compounds.

The phase stability plot shows a clear separation between stable and unstable compositions. Moreover, the fact that elements from the *s*,*d* and *f*-block are all accurately represented shows the wide applicability of this approach. All 1080 datapoints correspond to a unique composition, which can be found in the Supplementary material. Because of this high number, the predictive power of this approach will not significantly be increased by adding a few new compositions. Instead, the observed trend is compared with DFT calculations in the next section.

It is interesting to note the similarity between this plot and plots used in crystal structure prediction. They both separate two or more regions in phase space. For crystal structure prediction these regions represent two or more stable crystal structures, while in this case it separates stable from unstable compositions. The main difference is that the demarcation lines in crystal structure prediction plots have an arbitrary shape. For the phase stability plots however, the demarcation line can be described by an ellipse (see Supplementary information) showing a total probability of 94% based on the number of experimental/calculated datapoints inside/outside the ellipse, calculated by

$$P = \frac{n_{exp}^{in} + n_{calc}^{out}}{n_{total}}. \tag{3}$$

It has to be noted that the presence of *p*-block elements does not adversely affect these fractions, while they do adversely affect Fig. 2.

Because the plots are based on electronic properties, the shape of the ellipse can give insight into the electronic properties related to the crystal structure. The linear relationship in the plot is reflected in the rotation angle of the ellipse and gives information about the ratio between charge transfer and charge density mismatch. Apparently, this ratio is a crucial factor governing phase formation. The major and minor axes represent the tolerance in electron density mismatch and charge transfer, respectively. While the stability plot can also be constructed using the electronegativity and valence electron concentration to describe the electronic properties, the shape of the stability region does not allow the same reconstruction. In addition, the valence electron numbers are integers and are therefore less suited for this purpose. The atomic radii were found to show a correlation with $\Delta\Phi_w^*$ and $\Delta n_{WS,w}^{1/3}$ (see Supplementary information), allowing a 2D representation of the data.

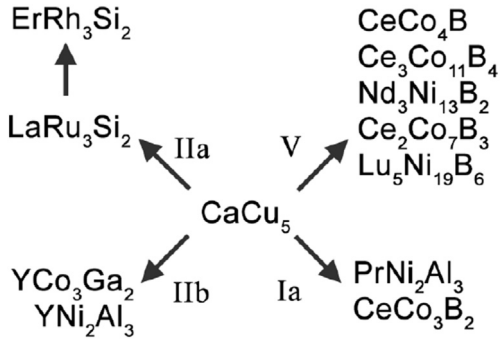

Fig. 6. Relationships between crystal prototypes. Modifications are: Ia ordered substitution, IIa internal deformation with reduction of symmetry, IIb with reduction of symmetry, III redistribution of atoms and V inhomogeneous homologous series (doubling of the unit cell).

3.3. DFT calculations

The proposed model uses the electronic properties of elemental solids and tries to capture the interactions in alloys. To see how well the model describes these interactions, DFT calculations were performed. A compound close to the center point of the ellipse was

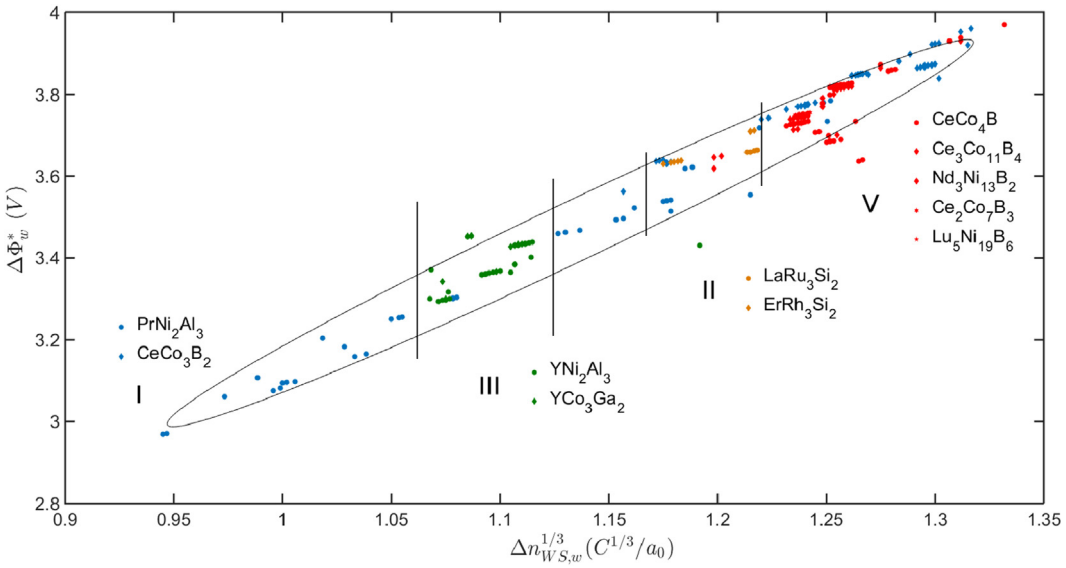

Fig. 7. The phase stability of $CaCu_5$ (indicated by the ellipse) and crystal modifications. Modification I is an ordered substitution and is found across the stability region. All other modifications (IIa/b internal deformation with/without reduction of symmetry, III redistribution of atoms and V doubling of the unit cell) are found to occupy a distinct part of the phase stability region and are governed by a substitution of *d*-metals by *p*-metals.

chosen as reference: YCu_5. The number of valence electrons was varied by substituting Cu by Fe, Co, Ni, Zn and Ga. The ionicity was varied by substituting Y by Mg, Ca, Sr and Ba. The 4 end members, YFe_5, YGa_5, $MgCu_5$, $BaCu_5$, are unstable while the other 6 compositions form a stable $CaCu_5$ phase. Although it should be noted that in addition the $CaCu_5$ prototype [28], a different crystal structure is reported for YZn_5 [29]. To compare the difference in work function, the charge q is calculated by integrating the electron density over half the (average) A-B distance. The charge difference is obtained relative to YCu_5. The average electron density at half the (average) A-B distance corresponds can directly be compared to $\Delta n^{1/3}_{WS,w}$. The comparison between the model and the DFT calculations is shown in Fig. 5.

The calculations show relative changes in the total charge and density at the boundary of the Wigner-Seitz cell compared to YCu_5. The plot shows large deviations for Fe and Mg based compounds, in line with the model. The relatively small deviation of $BaCu_5$ is enlarged in the DFT calculations, and shows that the model underestimates the charge transfer in Ba. YGa_5 follows the trend of the stable compounds, but has exceeded the tolerance limits.

3.4. Pseudo-binary crystal structures

The model can be extended to ternary crystal structures that are modifications of the $CaCu_5$-type crystal structure. The various modifications that can take place are shown in Fig. 6. The most common modification is an ordered substitution, where for $PrNi_2Al_3$ three B positions are occupied by elements possessing *p*-type valence electrons, while for $CeCo_3B_2$ only two B positions are replaced. Another modification is a superstructure formation, due to the substitution of a B atom for boron or silicon. There are five representatives of such a modification, each increasing the *c*-axis. A redistribution of atoms can also occur and this is the case for YCo_3Ga_2 and YNi_2Al_3 (substitution of B with Al or Ga). Finally, Si can distort the bond distances and angles, giving rise to $LaRu_3Si_2$ and to $ErRh_3Si_2$, where in the last case the symmetry is lowered to orthorhombic. This already indicates that the electrons show more localized behavior in these materials and that the Miedema model that assumes delocalized behavior will at one point break down.

Modification I does not change the symmetry of the system, but shows a preferential occupation of substituting atoms. This indicates that the average-atom model is no longer valid, because the atoms are not randomly distributed throughout the unit cell. However, the properties of the atoms at the two crystallographic sites are treated the same and does not result in differentiation phase space, as shown in Fig. 7. Modification II does change the symmetry of the system because of the M-Si interactions. This symmetry is a subgroup of the $CaCu_5$ symmetry, and it is expected that the phase stability region is also a subgroup of $CaCu_5$. Because these deformations are found in Si-containing systems, these compositions are found in a more narrow region in the stability plot. Modification III has a more profound effect on the unit cell dimensions and is found in another part of the stability region. Apparently, the interactions that give rise to this modification have a smaller tolerance. Modification V is only found in the presence of B, which also confines the stability parameters.

4. Conclusions

It is shown that by using the weighted Miedema parameters, a stability plot can be made, resembling plots used in crystal structure prediction. The plots have in common that they both model the charge transfer and electron density, but instead of using the electronegativity and valence electron number, the work function and electron density at the boundary of the Wigner-Seitz cell are used. By doing so, additional information about the factors that govern crystal structure formation can be obtained. In this case, the linear relationship between all stable compounds show a specific ratio between charge transfer and electron density. This observation is supported by DFT calculations. Not only does the empirical data show the boundary conditions for phase formation, it also allows the prediction of new stable compounds by linearly interpolating two binary compositions of interest. Although the nature of the valence electrons, being of *d* or *p* type, must be used with caution.

Acknowledgements

The authors like to thank J. Heringa, M. Sluiter R. Boom and F.R. de Boer for useful discussions. This work is part of an Industrial

Partnership Program of the Dutch Foundation for Fundamental Research on Matter (FOM) under IPP-i28, co-financed by BASF New Business. We acknowledge the Swedish Research Council (VR) and STandUP for the financial support and the Swedish National Infrastructure for Computing (SNIC) for computational resources.

Appendix A. Supplementary data

Supplementary data related to this article can be found at http://dx.doi.org/10.1016/j.jallcom.2017.06.134.

References

[1] Y. Zhang, Z.J. Zhou, J.P. Lin, G.L. Chen, P.K. Liaw, Solid-solution phase formation rules for multi-component alloys, Adv. Eng. Mater. 10 (6) (2008) 534–538.
[2] J.K. Liang, X.L. Chen, Q.L. Liu, G.H. Rao, Structures of rare earth-transition metal rich compounds derived from CaCu5 type, Prog. Nat. Sci. 12 (1) (2002) 1–9.
[3] Y. Hou, Z. Xu, S. Peng, C. Rong, J.P. Liu, S. Sun, A facile synthesis of SmCo5 magnets from core/shell Co/Sm_2 O_3 nanoparticles, Adv. Mater. 19 (20) (2007) 3349–3352.
[4] J.H.N. van Vucht, F.A. Kuijpers, H.C.A.M. Bruning, Reversible room-temperature absorption of large quantities of hydrogen by intermetallic compounds, Philips Res. Rep. 25 (133) (1970) 40.
[5] P. Villars, K. Cenzual, Pearson's Crystal Data: Crystal Structure Database for Inorganic Compounds, ASM International: Materials Park, Ohio, USA.
[6] A.F. Bialon, T. Hammerschmidt, R. Drautz, Three-parameter crystal-structure prediction for sp-d-valent compounds, Chem. Mater. 28 (8) (2016) 2550–2556.
[7] F.A. Mohammad, S. Yehia, S.H. Aly, A first-principle study of the magnetic, electronic and elastic properties of the hypothetical YFe_5 compound, Phys. B Condens. Matter 407 (13) (2012) 2486–2489.
[8] Y. Wang, J. Shen, N.X. Chen, J.L. Wang, Theoretical investigation on site preference of foreign atoms in rare-earth intermetallics, J. Alloys Compd. 319 (12) (2001) 62–73.
[9] F. Maruyama, H. Nagai, Y. Amako, H. Yoshie, K. Adachi, Magnetic properties of the hypothetical compound YFe_5, Phys. B Condens. Matter 266 (4) (1999) 356–360.
[10] A.R. Miedema, P.F. de Châtel, F.R. de Boer, Cohesion in alloys fundamentals of a semi-empirical model, Phys. B+C 100 (1) (1980) 1–28.
[11] Q. Guo, O.J. Kleppa, The standard enthalpies of formation of the compounds of early transition metals with late transition metals and with noble metals as determined by kleppa and co-workers at the university of chicago a review, J. Alloys Compd. 321 (2) (2001) 169–182.
[12] H. Zhang, S. Shang, J.E. Saal, A. Saengdeejing, Y.W.,L.Q. Chen, Z.K. Liu, Enthalpies of formation of magnesium compounds from first-principles calculations, Intermetallics 17 (11) (2009) 878–885.
[13] B. Zhang, W.A. Jesser, Formation energy of ternary alloy systems calculated by an extended Miedema model, Phys. B Condens. Matter 315 (13) (2002) 123–132.
[14] P.K. Ray, M. Akinj, M.J. Kramer, Applications of an extended Miedema's model for ternary alloys, J. Alloys Compd. 489 (2) (2010) 357–361.
[15] A.O. Lyakhov, A.R. Oganov, H.T. Stokes, Q. Zhu, New developments in evolutionary structure prediction algorithm uspex, Comput. Phys. Commun. 184 (2013) 1172–1182.
[16] A. Zunger, Systematization of the stable crystal structure of all ab-type binary compounds: a pseudopotential orbital-radii approach, Phys. Rev. B 22 (1980) 5839.
[17] P. Villars, A three-dimensional structural stability diagram for 998 binary AB intermetallic compounds, J. Less. Comm. Met. 92 (2) (1983) 215–238.
[18] D. Pettifor, Bonding and structure of intermetallics: a new bond order potential, Phil. Trans. R. Soc. Lond. A 334 (1991) 439–449.
[19] B. Cordero, V. Gomez, A.E. Platero-Prats, M. Reves, J. Echeverria, E. Cremades, F. Barragan, S. Alvarez, Covalent radii revisited, Dalton Trans. 21 (2008) 2832–2838.
[20] P. Hohenberg, W. Kohn, Inhomogeneous electron gas, Phys. Rev. B 136 (1964) 864.
[21] W. Kohn, L.J. Sham, Self-consistent equations including exchange and correlation effects, Phys. Rev. A 140 (1965) 1133.
[22] G. Kresse, J. Furthmüller, Efficiency of ab-initio total energy calculations for metals and semiconductors using a plane-wave basis set, Comput. Mat. Sci. 6 (1996) 15.
[23] G. Kresse, J. Furthmüller, Efficient iterative schemes for ab initio total-energy calculations using a plane-wave basis set, Phys. Rev. B 54 (1996) 11169.
[24] P.E. Blöchl, Projector augmented-wave method, Phys. Rev. B 50 (1994) 17953.
[25] G. Kresse, D. Joubert, From ultrasoft pseudopotentials to the projector augmented-wave method, Phys. Rev. B 59 (1999) 1758.
[26] J.P. Perdew, K. Burke, M. Ernzerhof, Generalized gradient approximation made simple, Phys. Rev. Lett. 77 (1996) 3865.
[27] C. Varvenne, A. Luque, W.G. Nöhring, W.A. Curtin, Average-atom interatomic potential for random alloys, Phys. Rev. B 93 (2016) 104201.
[28] E. Laube, J.B. Kusma, Über einige Y- und Dy-haltige legierungsphasen, Monatsh. für Chem. verwandte Teile anderer Wiss. 95 (6) (1964) 1504–1513.
[29] M.L. Fornasini, Crystal structure of (Ho-, Er-, Tm-, Lu-, Y-)Zn5 and ThCd5 intermetallic compounds, J. Less Common Metals 25 (3) (1971) 329–332.